CHAPTER - 5

Experimental and FE Analysis for the Post-Buckling Behaviour of Hat-Stiffened Panels under edge Compression Load

5.1 Introduction

The design of composite materials is aimed at achieving superior performance with specific strengths per unit weight. The stability design of stiffened panels is required to take into account compression, shear and combined compression-shear load cases. Under those load cases, the stiffened composite panels usually experience the local buckling of skin, stiffener buckling, global buckling and collapse. The failure of stiffened composite panel often starts from the interface between stiffeners and skin due to stress concentration induced by different deformation of the stiffeners and the skin after the local buckling of skin. The effect of the stiffener design and the skin thickness on the buckling resistance and post-buckling strength of stiffened composite panels was studied based on finite element (FE) method and experimental work.

Many experimental and numerical studies have been performed by various researchers on the pre-buckling and post-buckling behaviour on stiffened composite panels under axial compression. Most of the researchers have worked on the stiffened panels by using Blade-type, I-section, T- section and hat stiffeners. A very few literature is available on hat-type stiffener of panels. Kong et al. [19] studied analytically and experimentally on two stiffened panel configurations with I-shape and blade shape stiffeners. The buckling load and post-buckling behaviour of the panels was identified with application of strain gauge located at different locations by strain analysis. Bisagni and Cordisco [22] obtained experimental data from buckling and post-buckling tests performed until collapse on three

stiffened composite cylindrical shells. The buckling and post-buckling behaviour of stiffened composite panels were performed by experiment with different skin thickness and different T- shaped stiffener number [23-24]. Elaldi [26] studied of composite stiffened panels through experimentally and compared the post-buckling strength of structural efficiency of different types of the stiffened panels. Perret et al. [27] conducted the post-buckling test on composite panel and out-of-plane displacements were observed with application of two stereo Digital Image Correlation systems located on each side of the panel. Takeda et al. [29] presented buckling behaviour of fabricated two CFRP stiffened panels by VARTM. Buckling behaviour was investigated under compressive loading using FBG sensors and surface-attached strain gauges from impact test. Boni et al. [31] conducted experimental and numerical studies on the stiffened panel and compared FE analysis strains with strain gauges readings at mid-bay between the stringers, revealing a good prediction of the strain-load curves by which the buckling phenomenon is identified. The buckling load, buckling pattern failure load and failure mode were carried out on stiffened composite panel under the uniaxial compression load by experimental studies [33-34]. The numerical procedure for difficulties in setting the cohesive elements parameters was implemented in a commercial FEM software ABAQUS and adopted here to investigate the skin–stringer debonding growth in a stiffened composite panel subjected to compressive load [35-36]. The experimental studies have been carried out on graphite-epoxy blade stiffened composite panels subjected to axial compression load at the Aircraft Structures Laboratory of the Technion, Israel Institute of Technology and observed that all of the specimens were buckled at approximately the similar buckling strain [37]. Lanzi [39] carried out experimental studies on composite stiffened structures subjected to axial load for post-buckling behaviour, damage and failure mechanisms leading to collapse.

SudhirSastry et al. [47] presented the pre and post-buckling analysis of stiffened composite panels by ABAQUS based on the finite element method with CFC/epoxy, E-glass/epoxy and the Kevlar/epoxy composites material. It was determined that the initial geometric imperfections have more effect on the dynamic buckling of the shells, but the sensitivity to initial geometric imperfection depends on the ply configuration of the laminated shells [49, 50]. It has determined dynamic buckling loads of aluminum externally stiffened cylindrical shell structure with application of finite element and found that the initial geometric imperfections and half-wave sine shape load have prominent effect on the dynamic buckling of the shell structure [51]. It was observed that the imperfections lead to a significant reduction in the final collapse load of the complex steel silo transition junction structures but the amplitude of the imperfection has small influence on the collapse load of the structure [53, 54].

This chapter provides the buckling and post buckling response of composite stiffened panels through experimental studies and numerical analyses with application of ABAQUS. Non-linear finite element model is used to perform the post buckling behaviour of the panel with damage and debonding between the stiffener and composite panels.

5.2 Configurations of the Stiffened Composite Panel

The structural geometry of the laminated composite hat-stiffened panel is shown in Figure 5.1. Two specimens of panel are tested for experimental studies which are named with panel A and panel B. The laminated composite panel has been designed with two hat-stiffeners along the longitudinal direction as shown in Figure 5.2. The panel has a width of 400 mm and a length of 500 mm with 200 mm spacing and 35 mm depth of the stiffener with a top width of 25 mm. Ply configuration $[[45^0/\text{-}45^0/0^0/90^0/]_s]_s$ of 2 mm thickness of

skin laminated sheet has been used in all member of the hat-stiffened panel. The material property of each ply of thickness 0.125 mm is tabulated in Table 3.2.

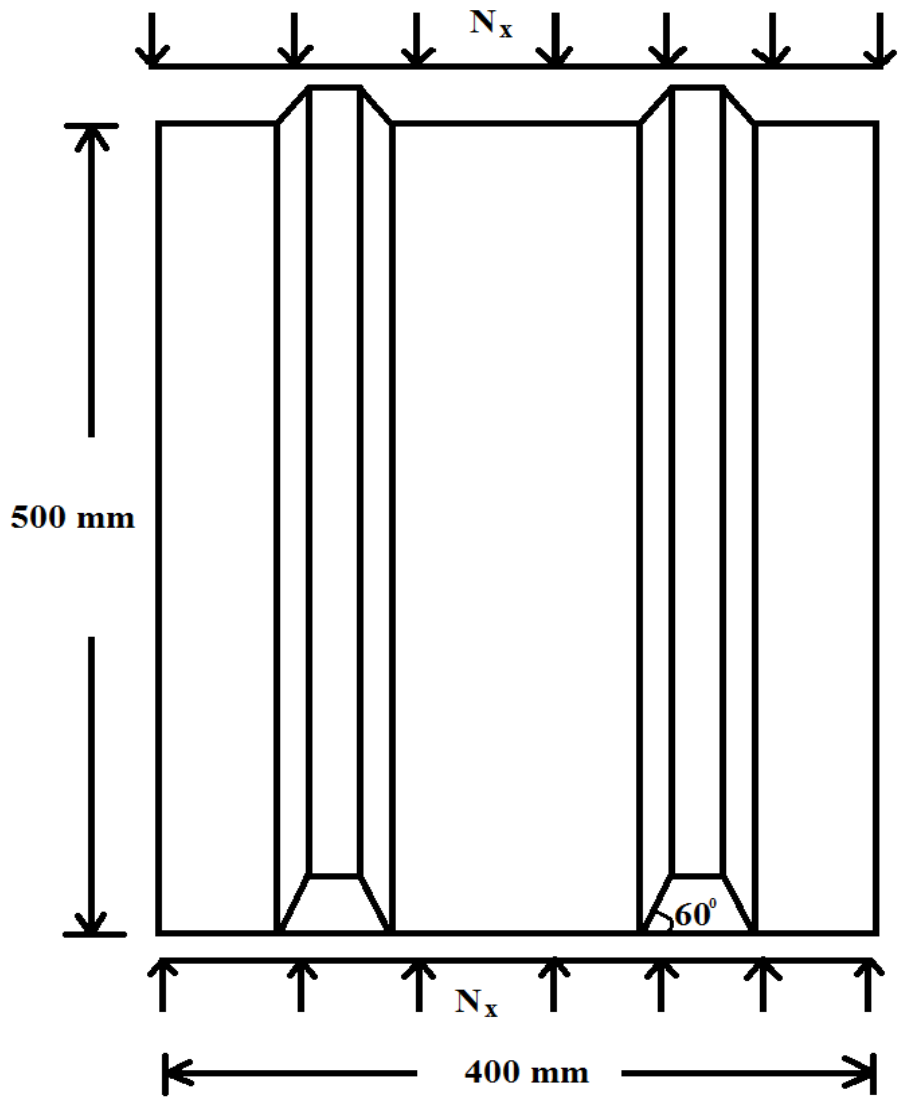

Figure 5.1 The structural geometry of the laminated composite 60^0-hat stiffened panel.

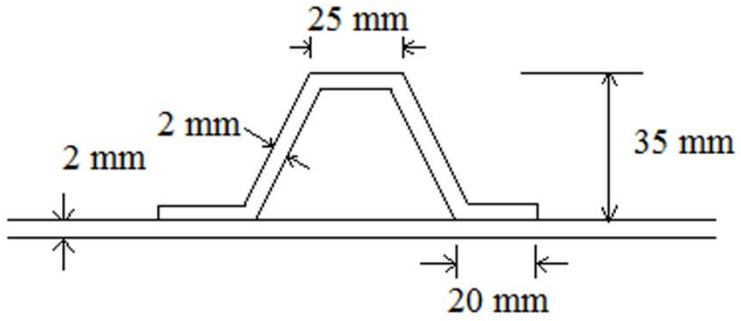

Figure 5.2 Cross-section of the hat-stiffener per pitch length.

5.3 Experimental Set Up

The uniaxial compression test on the stiffened composite panels have been performed by using a Universal Testing Machine setting with a maximum design capability of 400 kN with strain gauge data-logger system as shown in Figure 5.3. There are two steel platforms for the specimens loading. The bottom platform is moved in a controlled speed with hydraulic actuator, while the top platform is locked in a fixed location during the tests. The specimen has been installed on the test machine as shown in Figure 5.4. The panels were loaded with compressive load and clamped in loaded edges while the two unloaded edges of the panel were free. Before the experiment conducted, the location of specimen was adjusted to ensure that the panels were uniformly loaded. The compression tests were performed through controlling the loading rate of the hydraulic machine. In order to satisfy the ideal static test condition as much as possible during the loading process, the loading rate is controlled with 1 kN/s before the buckling of the hat-stiffened panel, and subsequently reduced to 0.5 kN/s during the post-buckling phase. The axial displacements of the panels were noted with increasing the compressive load.

Figure 5.3 Experimental set up of hydraulic machine with strain gauge data-logger system.

Figure 5.4 Specimen of hat-stiffened panel installation.

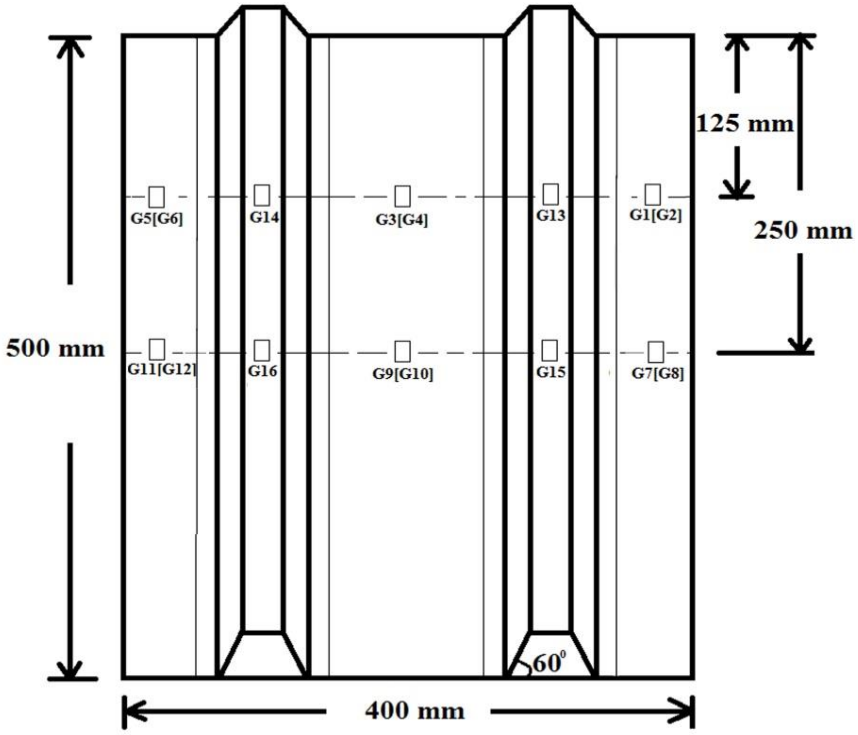

(a) Pattern-I

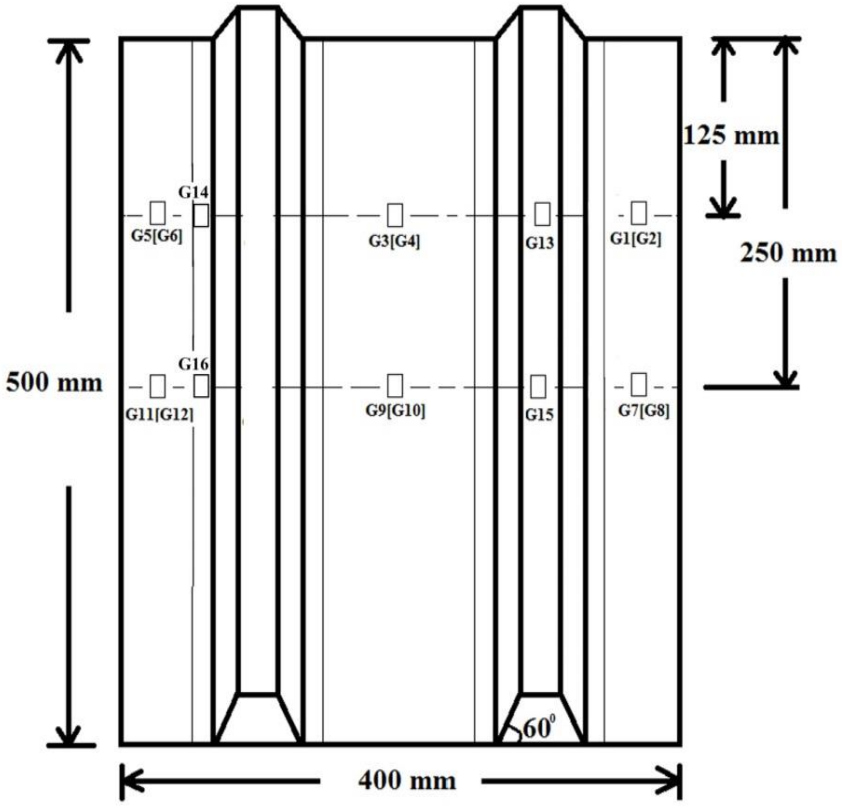

(b) Pattern-II

Figure 5.5 Locations of the strain gauges on panel.

The strain gauges were installed on the skin and stiffeners for monitoring the buckling status of the stiffened panel. A FE model was developed in ABAQUS/Standard to find the first and second buckling pattern of the stiffened panel for locating the strain gauges on the hat-stiffened panel. The strain gauges were located in two patterns for determination of behaviour of skin and stiffener as shown in Figure 5.5. 12 strain gauges (G1–G12) were located back-to-back on both sides of the skin to determine the membrane strains and the bending strains of skin when the buckling load reached. 4 strain gauges (G13–G16) were located on the hat-stiffener for determination of the behaviour of stiffeners.

5.4 Experimental Results

The first experiment has been conducted on specimen of panel-A. The cracking sound has been attended with increasing the load 265 kN/m. Finally, it is collapsed at load value of 274.7 kN/m by a loud noise. A visual damage can be observed near the skin-stiffener and debonding skin-stiffener of the panel as shown in Figure 5.6. Similar behaviour has been found for panel-B but failure load has been obtained 304.1 kN/m more than panel-A.

Figure 5.7 shows the load-axial displacement curve of the compressive tests on hat-stiffened panels. It is observed that the compressive load increases linearly up to 196 kN/m with increasing of the axial displacement of the panel. After that the rates of load increases corresponding to the axial displacement slow down until attending the collapse load of the panels. It is also observed that load carrying capacity of panel-A has lower than panel-B due to the difference of the damage areas and the manufacturing of the panel.

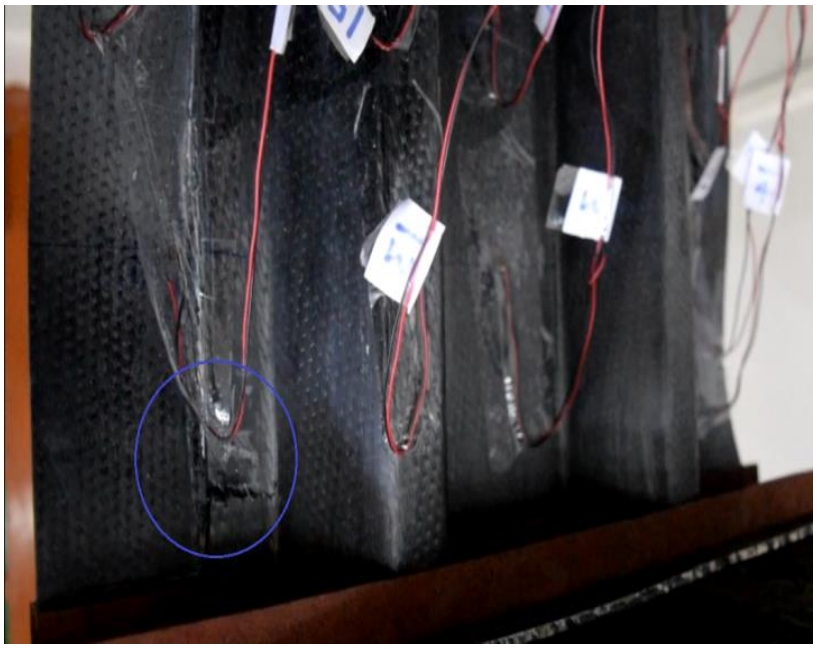

Panel – A

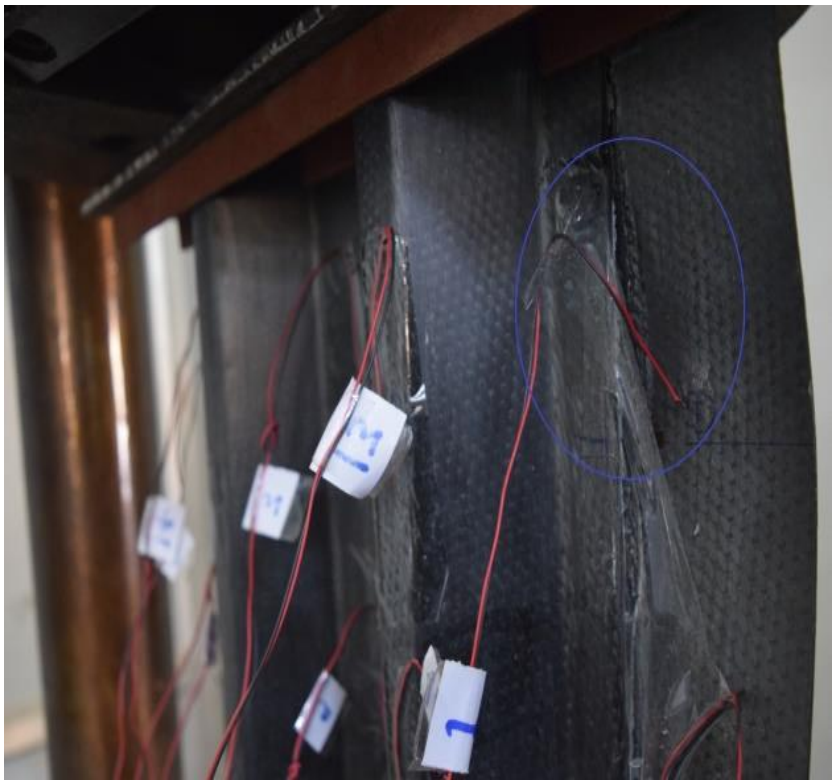

Panel – B

Figure 5.6 Failure mode of the panel.

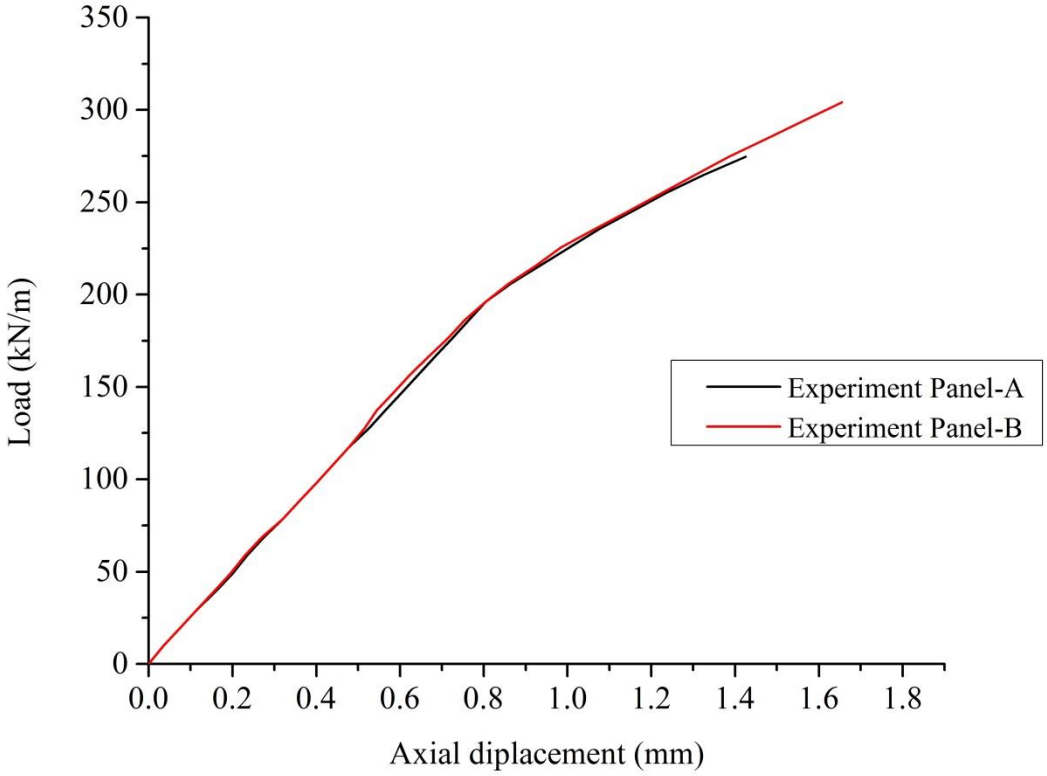

Figure 5.7 Load – axial displacement curves of experimental panel

The strain–load curves of strain gauges (G1–G6) have been presented for both stiffened panel as shown in Figure 5.8 to Figure 5.10. It is observed that the strain-load curves approximately linearly increases with increasing the load. Then the slopes of strain-load curves change suddenly in two opposite direction at quite close certain load value for different back-to-back strain gauges on the skin of the panels. This quite close certain load value can be easily found from Figure 5.8 to Figure 5.10, it can be said buckling load of the stiffened panel i.e. 196 kN/m. The buckling of the panels didn't occur simultaneously in different position of the stiffened panel due to damage areas, manufacturing defects of the panel and geometrical imperfections. It can be observed that the earliest buckling occurred at the strain gauge located on G6 of the panel-A with a compression load 190.5 kN/m. The

last buckling occurred at the strain gauge located on G2 of the panel-A with a compression load 196.3 kN/m.

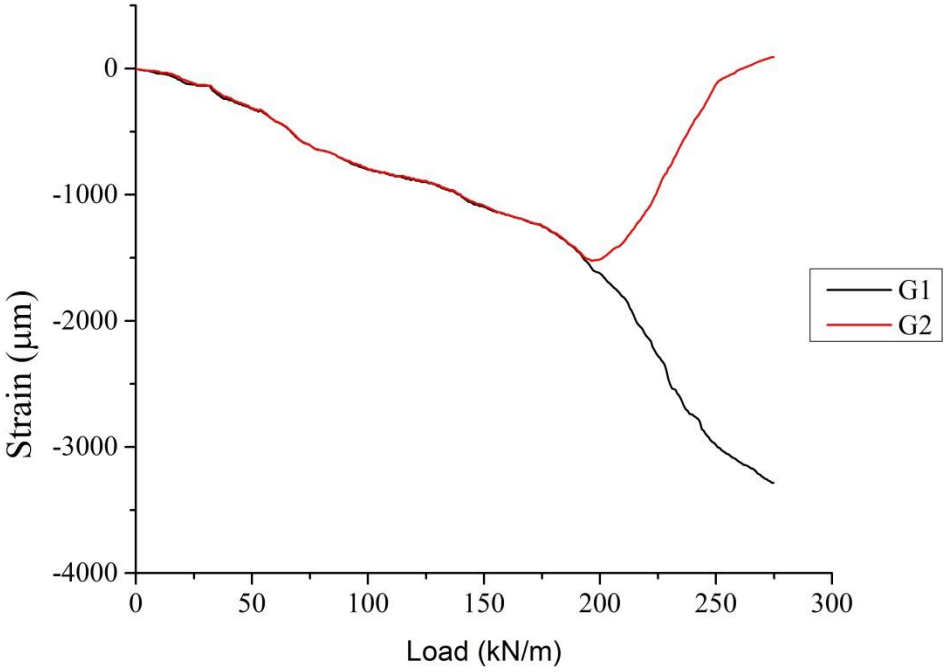

Panel – A

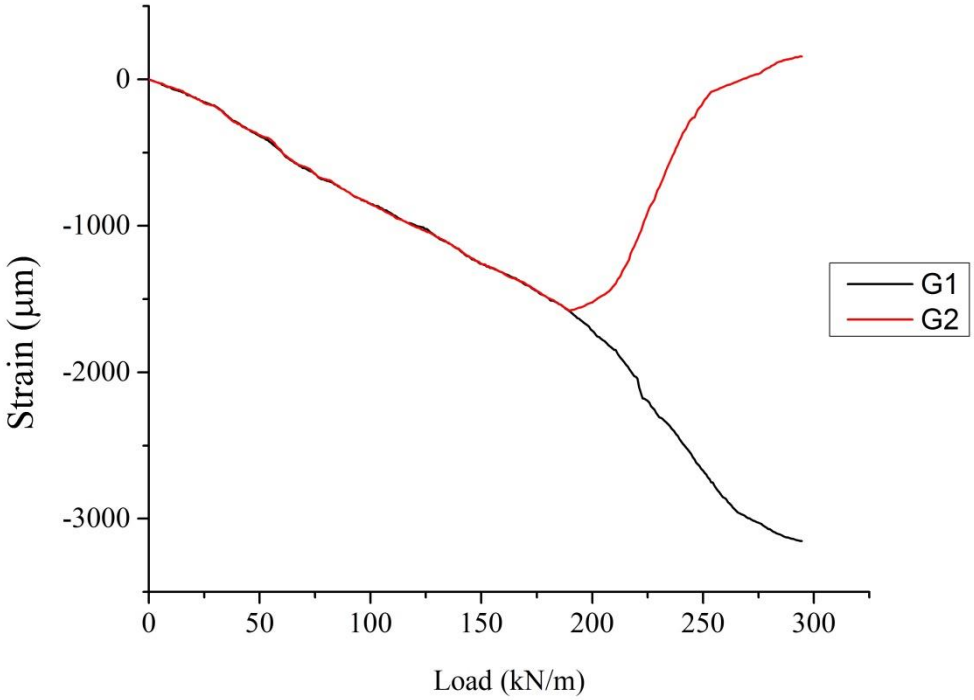

Panel – B

Figure 5.8 Strain-load curves of strain gauge G1 and G2

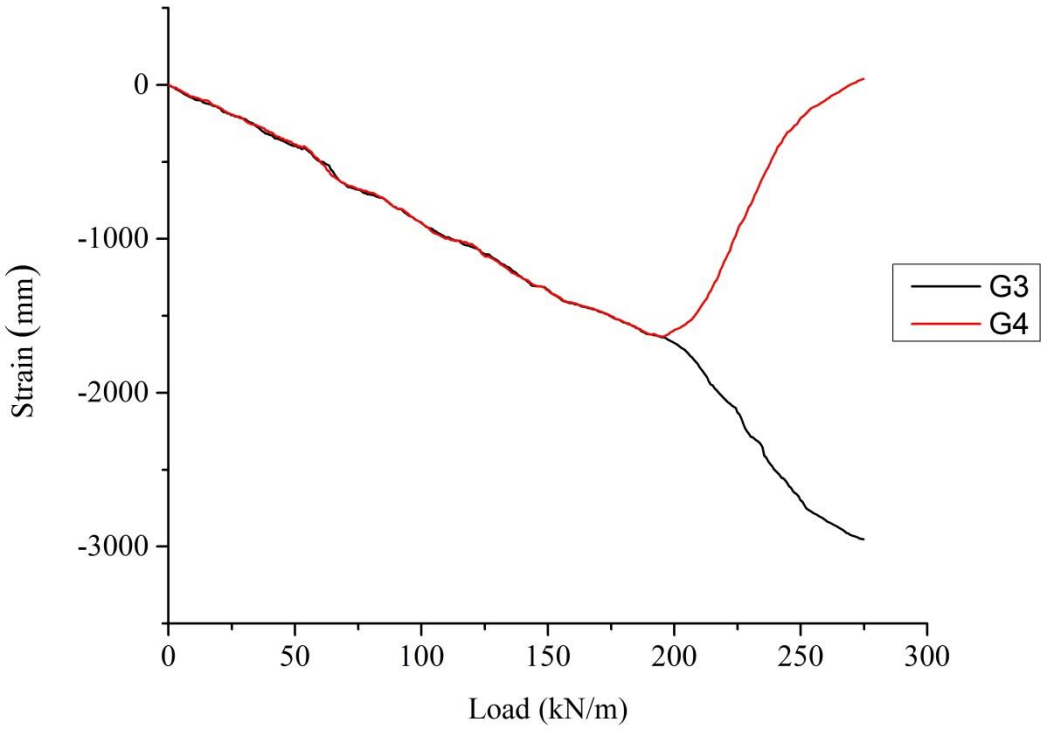

Panel – A

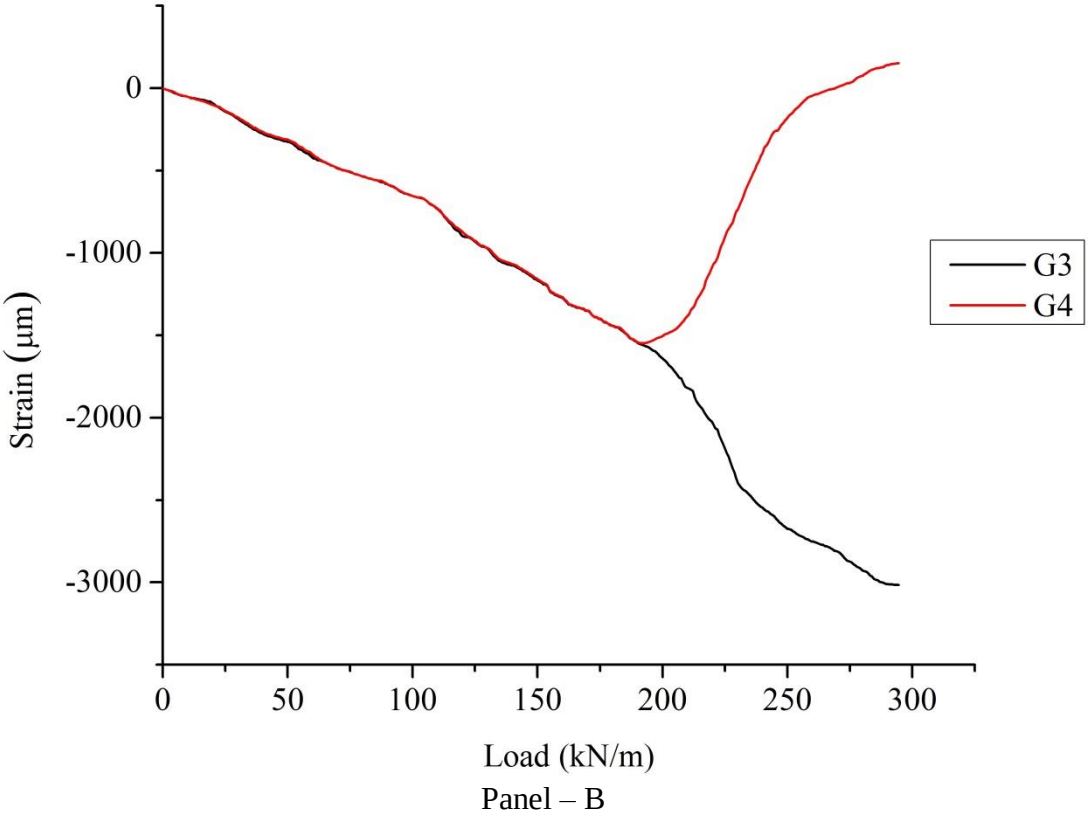

Panel – B

Figure 5.9 Strain-load curves of strain gauge G3 and G4.

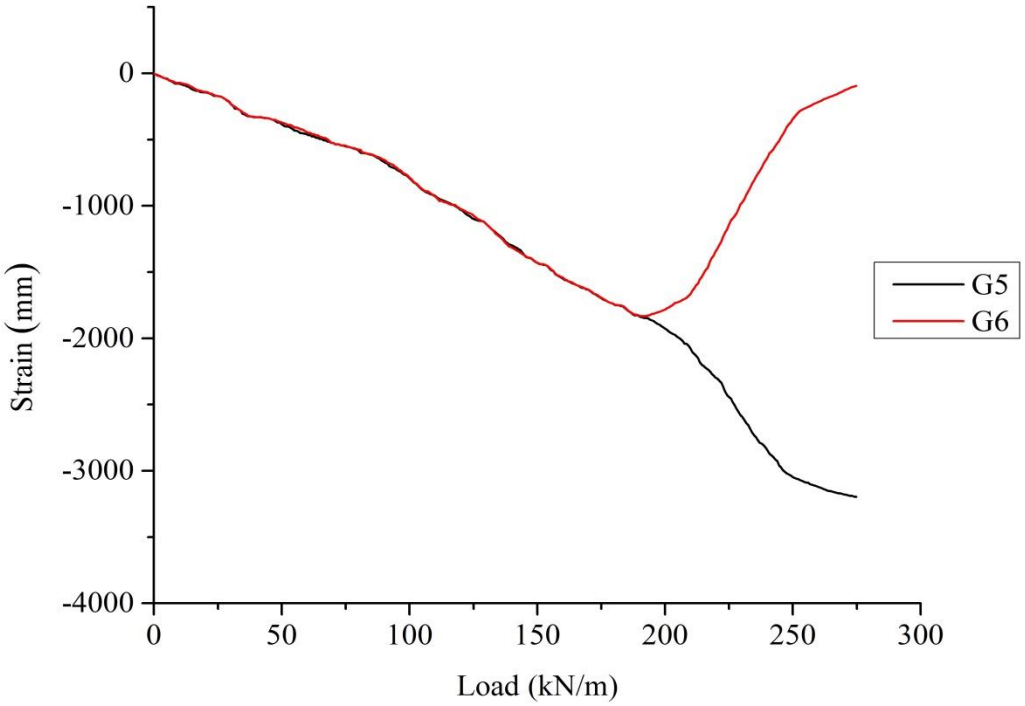

Panel – A

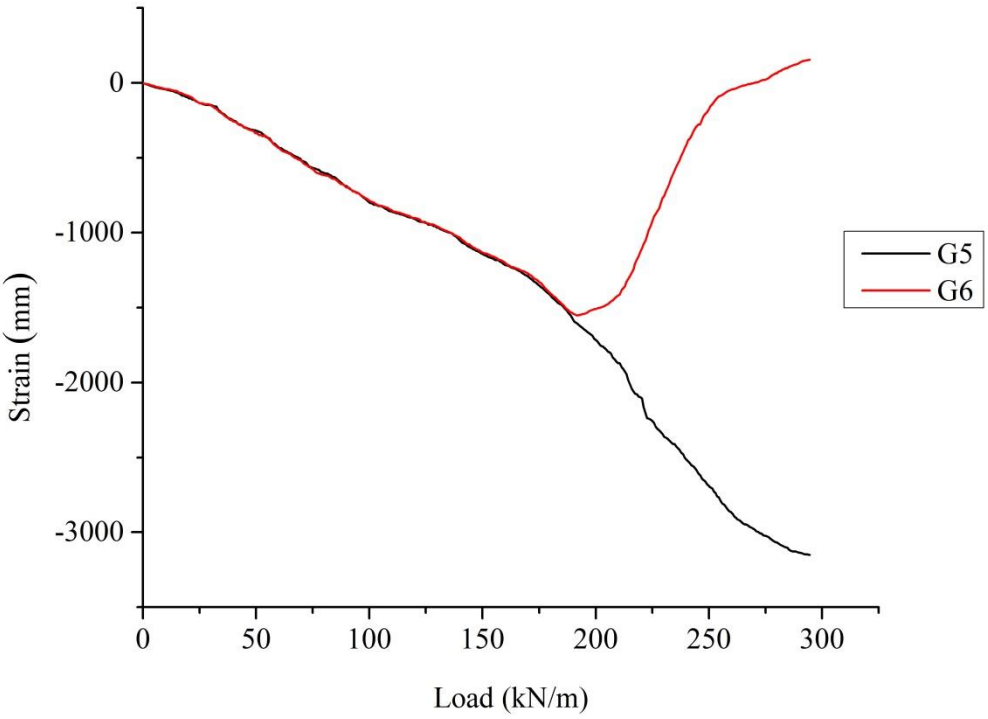

Panel – B

Figure 5.10 Strain-load curves of strain gauge G5 and G6.

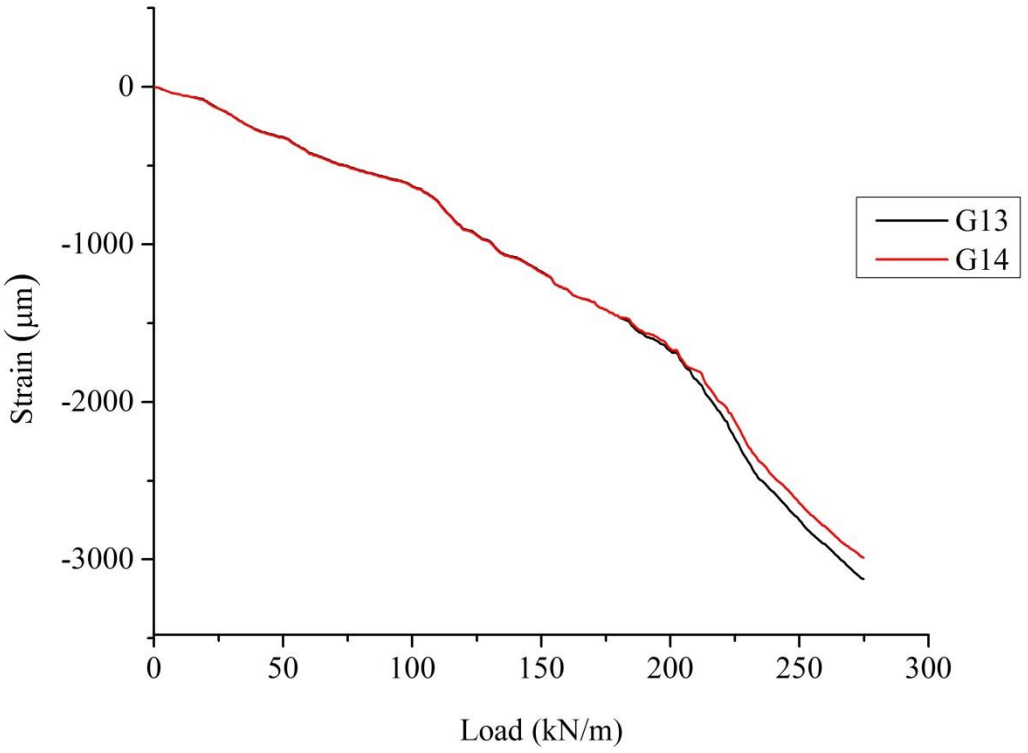

Panel – A

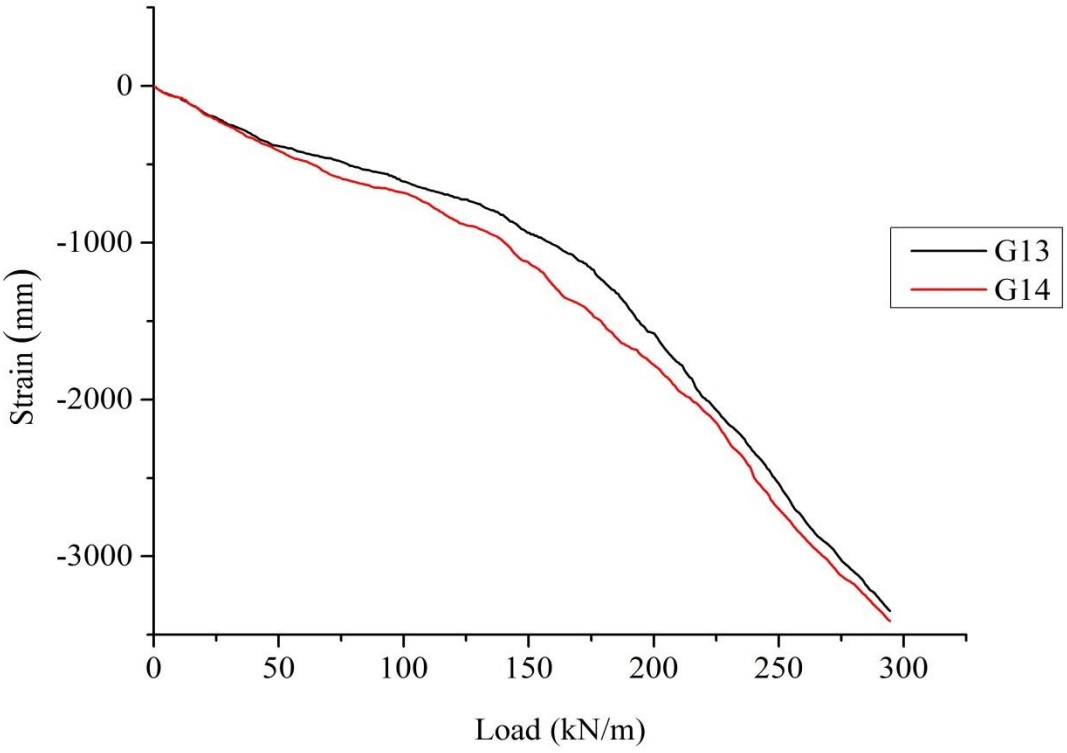

Panel – B

Figure 5.11 Strain-load curves of strain gauge G13 and G14.

Figure 5.11 shows the strain–load curves at different location on the panel, strain gauge G13 and G14 located at hat-stiffener upper flanges of the panel-A. However, for panel-B, G13 is located at hat-stiffener upper flanges panel-B but G14 is located at upper of skin-stiffener interface. It can be observed that the strain–load curves are slightly changed when the first buckling mode occurs. The reason behind this, the global stiffness of the laminated stiffened panel got reduced due to the local buckling of the skin. Thus, according to smeared stiffness ratio, the compression load will redistribute between plate of skin and hat-stiffeners of the panel. Hence, slopes of strain–load curves increases due to local buckling occurred near skin-stiffeners of the panel for strain gauges located on hat-stiffener upper flanges.

5.5 Non-Linear Finite Element Analysis

Non-linear buckling analysis has been performed with FE model of hat-stiffened panel by using ABAQUS. Shell element S4R is considered for analysis of thin panel which has both bending and membrane capabilities. The hat-stiffened panel is discretized with small global mess size of 5 mm and 12100 elements have bean generated of the stiffened panel as shown in Figure 5.12. Numerical studies have been performed on laminated composite stiffened panel made with CFC of ply configuration of $[[45^0/-45^0/90^0/0^0/]_s]_s$ with 2 mm thick laminated sheet in all member of panel as shown in Figure 5.1.

Firstly, the buckling analysis is studied using FE model to identify the buckling modes of the panel. The pre-buckling analysis is changed to perform a nonlinear FE analysis for post-buckling behavior of the panel. The post-buckling analysis has been performed with a Static Riks step in place of eigenvalue buckling step in ABAQUS. The geometric imperfections are allowed in smooth manner for the post-buckling analysis on

the basis of first four Eigen value buckling modes. The panel is loaded with axial compression and clamped in loaded edges and free in unloaded edges. The model is submitted for the post-buckling analysis and monitored continuously during the progress of bucking analysis.

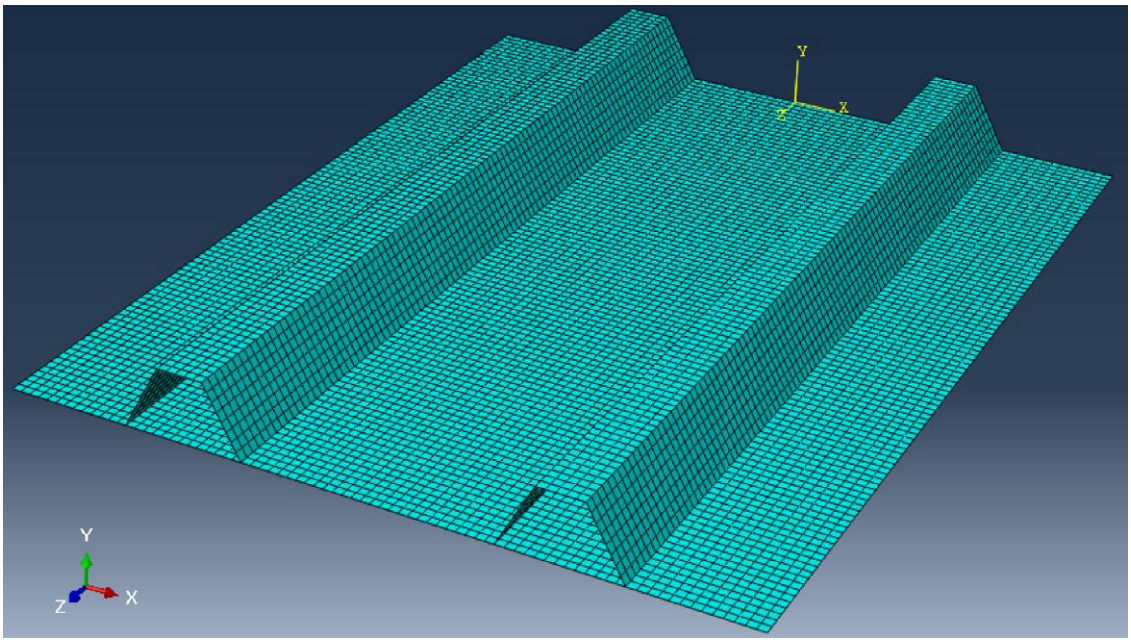

Figure 5.12 The panel discretized with shell element for finite element analysis.

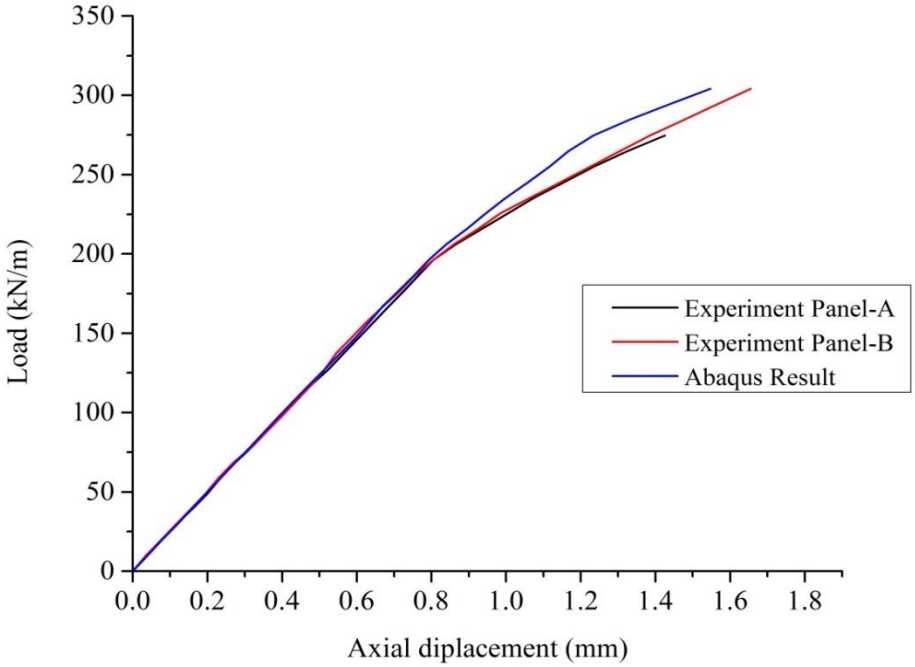

Figure 5.13 Load – axial displacement curves of experimental and simulated panel.

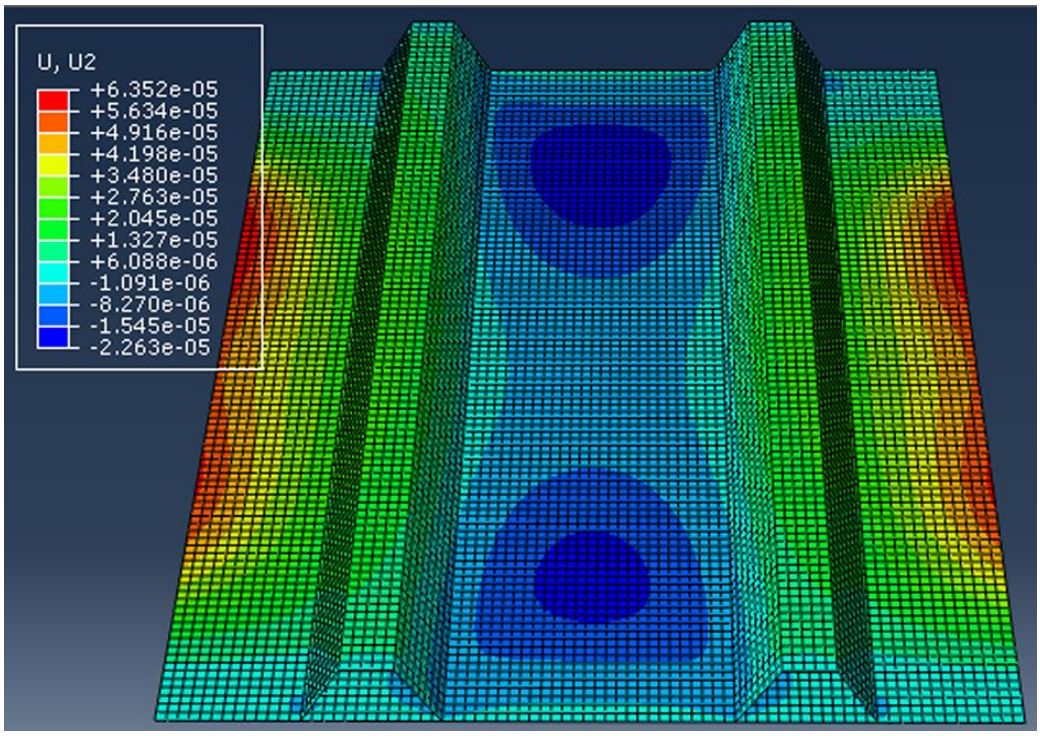

(a) Deformed patterns at load 98.1 kN/m load

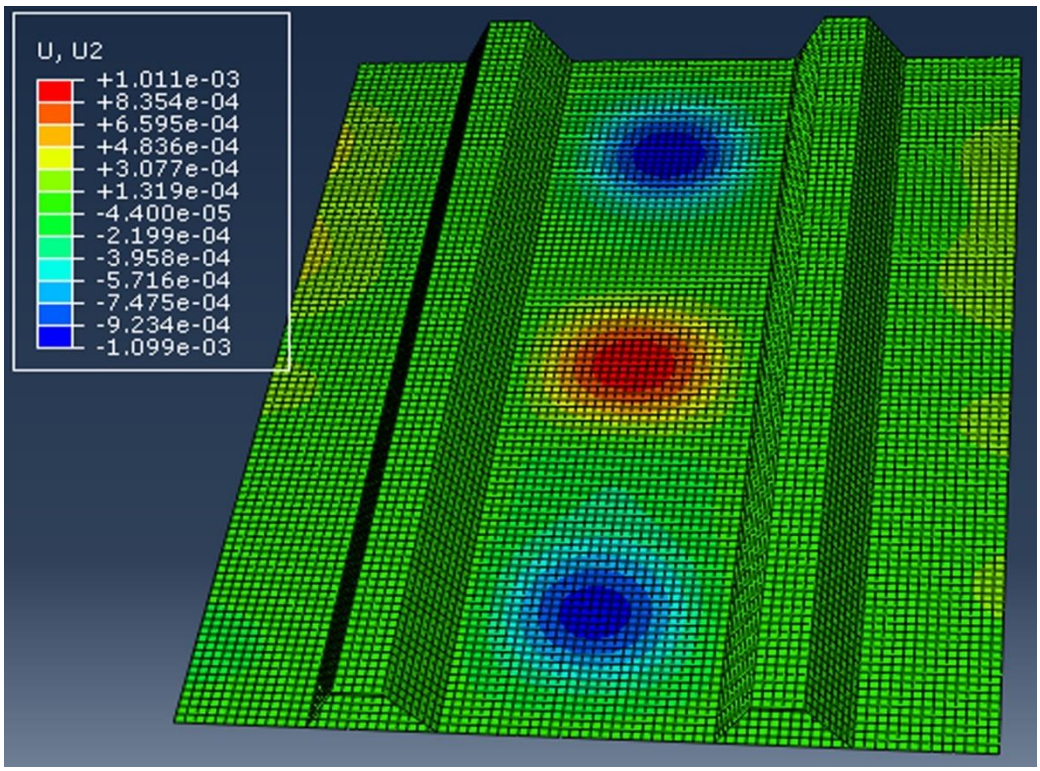

(b) Deformed patterns at 206.01 kN/m load

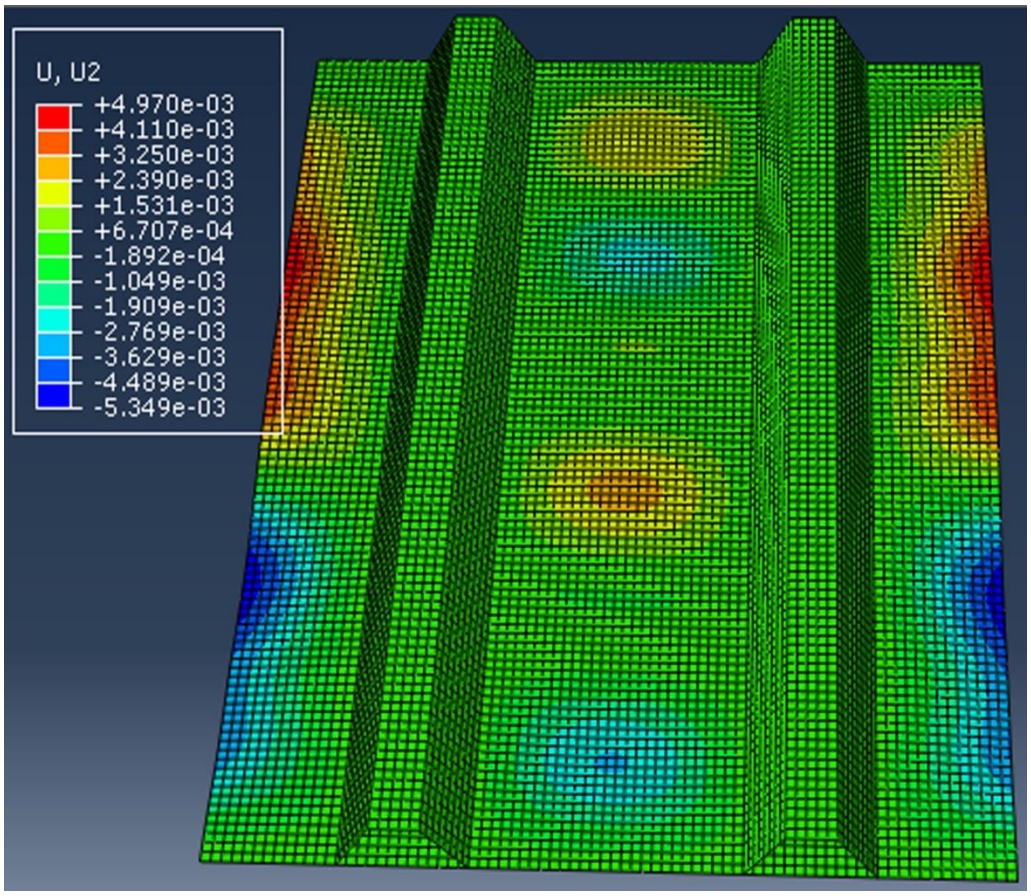

(c) Deformed patterns at 304.1 kN/m load

Figure 5.14 The out of plane displacement pattern at different load for FE analysis.

Hashin's damage initiation criterion has implemented to predict the onset of damage in the post-buckling analysis. A stiffness reduction method [25] was applied and further loading caused a complete loss of stiffness, when the damage initiation criterion was satisfied. The damage evolution law is based on the fracture energy dissipated throughout damage process. The elastic properties and the strength properties for Hashin's damage initiation criteria are given in Table 3.2.

Figure 5.13 shows the compressive load-axial displacement curve of stiffened panel together with simulated FE model results and the experimental results. It is observed that the curve of compressive load vs. axil displacement is straight then it is inclined after

increase of compression load. The axial displacement of the panel obtained through experiment is more than the axial displacement found from the damage model due to presence of the implanting material, such as epoxy, in the supported ends of the panel. Therefore, results are normalized using the axial displacement at the buckling load. From compression load vs. axial displacement curve, the critical buckling load and critical displacement of the stiffened panel is obtained as 206 kN/m and 0.839 mm respectively. Figure 5.14 shows the out of plane displacement pattern of the panel at different specific loads which are taken from load-axial displacement curve shown in Figure 5.13. The out of plane displacement pattern shows that the compression failure originated at edges of the panel and gone to skin-stiffener bonding. Finally, failure of the stiffened panel happened due to debonding between skin-stiffener.

5.6 Summary

In this chapter, the pre-buckling and post buckling has been conducted on the hat-stiffened panel under in-plane compression load by experiments. And also non-linear buckling analysis on the hat-stiffened panel under in-plane compression load has been performed by using FE software ABAQUS. The experiments results have been found on two hat-stiffened panels with equally spaced stiffeners. The buckling behaviour of the panel has been determined with application of finite element model by using ABAQUS and compared with experimental results. The compressive load-axial displacement curve of the experiments has good agreement with simulated FE model result for prediction of the buckling behaviour of the panel up to the failure load. The local buckling of skin has been observed before the buckling of the panel from strain analysis at different locations. A visual damage has found near the skin-stiffener and debonding skin-stiffener of the panel

during failure of the hat-stiffened panel. The failure load of the panel is approximately 1.5 times of the buckling load for experiments study of the panel. The simulated FE models result shows that the failure load of the panel is about 2 times of the buckling load of the panel. The out of plane displacement pattern indications that the compression failure originated at edges of the panel and gone to skin-stiffener bonding. And finally failure of the panel happened due to debonding between skin-stiffener.